AD

TECHNICAL REPORT ARCCB-TR-98020

COMPREHENSIVE EROSION MODEL FOR THE 120-MM M256/M829 GUN SYSTEM

S. SOPOK
P. VOTTIS
P. O'HARA
G. PFLEGL
C. RICKARD

DECEMBER 1998

US ARMY ARMAMENT RESEARCH,
DEVELOPMENT AND ENGINEERING CENTER
CLOSE COMBAT ARMAMENTS CENTER
BENÉT LABORATORIES
WATERVLIET, N.Y. 12189-4050

APPROVED FOR PUBLIC RELEASE; DISTRIBUTION UNLIMITED

DISCLAIMER

The findings in this report are not to be construed as an official Department of the Army position unless so designated by other authorized documents.

The use of trade name(s) and/or manufacturer(s) does not constitute an official endorsement or approval.

DESTRUCTION NOTICE

For classified documents, follow the procedures in DoD 5200.22-M, Industrial Security Manual, Section II-19, or DoD 5200.1-R, Information Security Program Regulation, Chapter IX.

For unclassified, limited documents, destroy by any method that will prevent disclosure of contents or reconstruction of the document.

For unclassified, unlimited documents, destroy when the report is no longer needed. Do not return it to the originator.

REPORT DOCUMENTATION PAGE

Form Approved
OMB No. 0704-0188

1. AGENCY USE ONLY *(Leave blank)*	2. REPORT DATE	3. REPORT TYPE AND DATES COVERED
	December 1998	Final

4. TITLE AND SUBTITLE
COMPREHENSIVE EROSION MODEL FOR THE
120-MM M256/M829 GUN SYSTEM

5. FUNDING NUMBERS
AMCMS No. 6226.24.H180.0
PRON No. 4A8A8FYK1ABJ

6. AUTHOR(S)
S. Sopok, P. Vottis, P. O'Hara, G. Pflegl, and C. Rickard

7. PERFORMING ORGANIZATION NAME(S) AND ADDRESS(ES)
U.S. Army ARDEC
Benet Laboratories, AMSTA-AR-CCB-O
Watervliet, NY 12189-4050

8. PERFORMING ORGANIZATION REPORT NUMBER
ARCCB-TR-98020

9. SPONSORING / MONITORING AGENCY NAME(S) AND ADDRESS(ES)
U.S. Army ARDEC
Close Combat Armaments Center
Picatinny Arsenal, NJ 07806-5000

10. SPONSORING / MONITORING AGENCY REPORT NUMBER

11. SUPPLEMENTARY NOTES
Presented at the 1998 JANNAF Propulsion Meeting, Cleveland, OH, 15-18 July 1998.
Published in proceedings of the meeting.

12a. DISTRIBUTION / AVAILABILITY STATEMENT
Approved for public release; distribution unlimited.

12b. DISTRIBUTION CODE

13. ABSTRACT *(Maximum 200 words)*

Most 120-mm M256 guns firing the M829 round as their "hottest" kinetic energy round have been condemned because of fatigue. Despite this fact, it is still important to determine the erosion life of the M829 round, since M256 guns that have fired the most recent kinetic energy rounds (M829A1, M829A2) rely on the M829 round for baseline dispersion testing of that gun. Today this generally results in M256 guns that having an equal mix of M829 and M829A2 rounds, thus necessitating the consideration of M829 round effects for any erosion analysis. Variability exists for M256 guns with M829 rounds depending on round count, round type, round-conditioning temperature, and their order. Distinctive erosion patterns and mechanisms are emerging as our gun erosion database increases for in-service and out-of-service 120-mm M256 tubes with M829 rounds. Our M256/M829 gun system erosion model—with its interior ballistics, thermochemistry, and boundary layer components—is constantly being guided and refined by the erosion and materials analysis data from fired gun tubes. A recent refinement includes improvement of the gun steel subsurface exposure model due to high quality, difficult to obtain data from in-service M256 tubes. Other recent refinements to the boundary layer heat transfer model are based on thermal data from M256 tubes. These refinements include the improvement/incorporation of case gas cooling effects, turbulent gas mixing/heating effects, and a very minor contribution from forcing cone-induced vena contracta cooling effects. These latter refinements are calibrated away from crack walls by positional thermal wall repacking depth, thermal wall transformation depth, and thermocouple data. A comprehensive gun erosion model and multiple single-shot erosion condemnation predictions are described for the 120-mm M256 gun with its M829 round for hot-conditioned rounds only, ambient-conditioned rounds only, cold-conditioned rounds only, and an equal distribution of hot/ambient/cold-conditioned rounds. The gun erosion mechanism consists of heat checking of the inert chromium plate, subsequent interfacial degradation of the subsurface gun steel substrate at the chromium crack bases, then subsequent chromium platelet spalling, and subsequent bare gun steel gas wash. This gun erosion model correctly calculates and predicts that the worst eroded region is at 1.2 to 2.4 meters from the rear face of the tube. The excessive muzzle wear is by a different, purely mechanical gas wash-free mechanism. Most importantly, given herein are the relative erosion related effective full-charge values of the fielded M256 gun kinetic energy rounds at various round-conditioning temperatures.

14. SUBJECT TERMS	15. NUMBER OF PAGES
Gun Erosion Modeling, 120-mm M256 Cannon, M829 Rounds	22
	16. PRICE CODE

17. SECURITY CLASSIFICATION OF REPORT	18. SECURITY CLASSIFICATION OF THIS PAGE	19. SECURITY CLASSIFICATION OF ABSTRACT	20. LIMITATION OF ABSTRACT
UNCLASSIFIED	UNCLASSIFIED	UNCLASSIFIED	UL

TABLE OF CONTENTS

LIST OF ILLUSTRATIONS

INTRODUCTION

Both U.S. Army experimental data and numerous ADPA Tri-Service sponsored gun erosion meetings have implied a thermal-chemical-mechanical gun barrel erosion mechanism (refs 1,2). A unified computer model for predicting thermal-chemical-mechanical erosion in gun barrels was first described by Dunn et al. in 1995 (ref 3) using the following codes:

- Standard heat transfer modified by mass addition to boundary layer rocket code modified for guns (MABL)
- Standard nonideal gas-wall thermochemical rocket code modified for guns (CCET)
- Standard wall material ablation conduction erosion rocket code modified for guns (MACE)

Additionally, this gun barrel erosion model requires the standard interior ballistics gun code (XNOVAKTC) (ref 4) for input. To the degree available, our practical approach to gun barrel erosion modeling is kept on-track with actual experimental gun system data. As our gun erosion database increases, our gun erosion model evolves to include identifiable patterns.

The purpose of this report is to describe our comprehensive gun erosion model for the 120-mm M256 gun with its M829 round. In addition, we have included detailed erosion condemnation predictions for four single-shot firing scenarios.

PROCEDURE

For the 120-mm M256 gun with its M829 round, a comprehensive gun erosion model was developed that requires many types of experimental data to keep this gun erosion model on-track. These data include:

- Pressure gauge
- Radar
- Thermal repacking (recrystallization) depth away from cracks (chromium plate, ~1300°K)
- Thermal transformation depth away from cracks (gun steel, ~1000°K)
- Thermocouple
- Kinetic rate function
- Subsurface metallographic and borescope data

Initial 120-mm M256/M829 gun system erosion modeling included the XNOVAKTC interior ballistic analysis for gas pressure, gas temperature, and gas velocity core flow data at hot (49°C), ambient (21°C), and cold (-32°C) round-conditioning temperatures (ref 4). The MABL boundary layer recovery enthalpy/cold wall heat flux analysis and the CCET thermochemistry inert wall enthalpy/reacting wall enthalpy/ablation potential analysis (ref 3) followed this initial step. The final step included the MACE wall temperature/erosion profile analysis (ref 3). Specifically, detailed M256/M829 erosion condemnation predictions were formulated for four single-shot firing scenarios including hot-conditioned rounds only, ambient-conditioned rounds only, cold-conditioned rounds only, and an equal distribution of hot/ambient/cold-conditioned rounds.

RESULTS AND DISCUSSION

Figure 1 summarizes the M829 XNOVAKTC interior ballistic analysis for maximum values of gas pressure (P_g), gas temperature (T_g), and gas velocity (V_g) as a function of axial position and round-conditioning temperature. Maximum values were used instead of time-dependent data to simplify the appearance of this figure. Selected axial positions included 0.69, 1.55, 2.18, 3.30, and 5.11 meters from the rear face of the tube (RFT), while the selected round-conditioning included hot (49°C), ambient (21°C), and cold (-31°C) temperatures. (These five selected axial positions and three selected round-conditioning temperatures will be used exclusively for the rest of the figures in this report). Experimental pressure-time and muzzle velocity data were used to calibrate the interior ballistic analysis. In Figure 1, the T_g and P_g values decrease with increasing axial position, while the V_g values increase with increasing axial position for the bore region.

Figure 2 summarizes the M829 MABL analysis for maximum values of recovery enthalpy (H_r) and cold wall heat flux (Q_{cw}) as a function of the selected axial positions and round-conditioning temperatures. Maximum values were also used instead of time-dependent data to simplify the appearance of this figure. Experimental thermal repacking depth away from cracks, thermal transformation depth away from cracks, and thermocouple data were used to calibrate this improved boundary layer analysis. The figure illustrates that H_r and Q_{cw} values increase with increasing axial position for the 0.6 to 1.2 meter from RFT region; both values peak in the 1.2 to 2.4 meter range; then both values decrease with increasing axial position to the muzzle. Note that the heat transfer pattern in Figure 2 significantly differs from the core flow pattern in Figure 1 and cannot be explained solely on the basis of simple heat transmission (film) coefficient effects (ref 5). We theorize that this difference can be explained by an improved boundary layer analysis, including significant combustion case gas cooling effects and these significant turbulent gas mixing/heating effects.

Without combustion case gas cooling effects and turbulent gas mixing/heating effects, the 0.6 to 1.2 meter region would be the highest wall heat transfer region, but with both of these effects, the 1.2 to 2.4 meter region is the highest wall heat transfer region. The combustion case gas cooling effect is similar to transpiration, slot injection, and pure fuel injection cooling at the wall for rocket chambers, as well as ablative cooling at the wall for guns.

Combustible case gases were approximately 1600°K maximum for the M829 round, while propellant core flow gases were approximately 3000°K maximum for this round. The combustible case ablates and its cooler gases (compared to the core flow) stay along the wall providing a cooled boundary layer from the onset of the bore at 0.6 meter from RFT to where it changes over to highly turbulent in the 1.2 to 2.4 meter from RFT region. This cooling reduces heat transfer to the wall and diminishes with increasing axial position. For the bore region, the increasingly turbulent boundary layer is due to geometry and flow field conditions that are characterized by a transition from turbulent microscopic fluid mixing to highly turbulent macroscopic fluid mixing.

A combination of M256/M829 chamber, forcing cone, and bore geometry induce a very minor vena contracta flow from the 0.6 meter from RFT onset of the bore to the 1.2 to 2.4 meter from RFT region. This type of flow exhibits slightly slower velocities in the boundary layer, thus slightly reducing heat transfer to the wall, then diminishing with increasing axial position.

Figure 3 summarizes the M829 CCET thermochemical analysis of reacting wall enthalpy (H_w) and ablation potential (B_a) (ref 3) as a function of the wall temperatures (T_{wall}) for high contraction (HC) chromium plate/A723 gun steel wall materials. Experimental kinetic rate function data and subsurface metallographic data were used to calibrate the thermochemical analysis and transform the chemical equilibrium analysis into a partial chemical kinetic analysis. The HC chromium maximum T_{wall} is about 1600°K for the M256/M829 gun system. This is below its passivating oxidation temperature at about 2000°K and well below its melting point at about 2130°K, which explains its inertness. The A723/iron maximum T_{wall} is about 1375°K for the M256/M829 gun system. This is well above its rapid expansive flaking oxidation temperature at about 1055°K, explaining its reactivity. In addition, it is below its iron oxide melting point at about 1640°K and well below its A723/iron melting point at about 1810°K.

Figure 4 summarizes the M829 borescope data analysis of the A723 subsurface exposure through HC chromium plate cracks as a function of rounds fired for selected axial positions. The experimental borescope data was used to calibrate the erosion analysis. This data was collected on a cleaned M256 tube that had mostly M829 rounds. These M829 rounds consisted of a nearly equal distribution of hot/ambient/cold temperature conditioning. Data collection involved the use of a magnifying borescope with a calibrated scale to measure the number and average area of each HC chromium platelet within a designated total area as a function of axial position for a given round count.

We were able to collect high quality borescope data on a single M256 tube with mostly M829 rounds near its 50-round point, near its 200-round point, and at its final out-of-service round point. The balance of the non-M829 rounds was converted to effective M829 rounds. The initial zero-round condition data were not collected from this M256 tube, but from the many unfired M256 tubes available at Watervliet Arsenal. High contraction chromium plate has fine cracking and finite shrinkage when manufactured and prior to firing. We recognize that this is a sample of one and that significant variability exists depending on combinations of round count, round type, round-conditioning temperature, and their firing order.

For the selected axial positions in Figure 4, from 50 to 150 rounds, A723 subsurface exposure rose rapidly due to HC chromium thermal repacking, nonmetallic out-gassing, and possibly compression resulting in its shrinkage and heat checking. After about 150 rounds, the above mechanism diminished and the A723 subsurface exposure rose more slowly because only the HC chromium platelet spalling mechanism remained. At the 5.11 meter from RFT near-muzzle position, the A723 subsurface exposure rose very rapidly from about 150 rounds until its out-of-service round count due to HC chromium platelet spalling by a different purely mechanical mechanism. This tube was condemned due to fatigue at its full fatigue life.

Figure 5 (top) presents a typical 100x metallograph of an M256 tube with mostly M829 rounds at 0.69 meter from RFT. This represents the 0.6 to 1.2 meter region and was used to calibrate the erosion analysis. The 0.6 to 1.2 meter region has the highest gas pressure of any bore region (Figure 1), which explains the deep crack depths due to severe dilation. Although this 0.6 to 1.2 meter region has the highest gas temperature of any bore region (Figure 1), heat transfer to the wall is significantly diminished due to combustion case gas cooling effects (Figure 2). These observations explain the heat checking and crack spacing as well as the near absence of interface degradation and chromium platelet spalling.

Figure 5 (bottom) presents a typical 100x metallograph of an M256 tube with mostly M829 rounds at 1.55 meters from RFT. This represents the 1.2 to 2.4 meter region and was also used to calibrate the erosion analysis. The 1.2 to 2.4 meter region has a lower gas pressure than the 0.6 to 1.2 meter region (Figure 1), which explains the moderate crack depths due to moderate dilation. Although this 1.2 to 2.4 meter region has a lower gas temperature than the 0.6 to 1.2 meter bore region (Figure 1), heat transfer to the wall is significantly higher due to turbulent gas mixing (Figure 2). These observations explain the heat checking and crack spacing as well as the noticeable interface degradation and mild chromium platelet spalling. We theorize that the main gun erosion mechanism consists of inert chromium plate cracking, shrinkage, and heat checking, followed by subsequent interfacial degradation of the subsurface gun steel substrate at the chromium crack bases, subsequent chromium platelet spalling, and subsequent bare gun steel gas wash. The gun steel at the chromium/gun steel interface is more susceptible to interface degradation than either of its components separately due to its higher energy state and reactivity. In addition, interface degradation is enhanced by expansive flaking of iron oxide.

As chromium platelets detach from the substrate and rise above attached chromium platelets, they are more susceptible to mechanical removal by the projectile. In addition, the 1.2 to 2.4 meter region has a wavy chromium surface appearance in cross-section due to partially detached chromium platelets. Rarely do radial heat-checking cracks link-up to spall a chromium platelet with attached gun steel. Although there appears to be evidence of heat-checking cracks extending into the wall well beyond the heat-affected zone due to environmental-assisted cracking, great scrutiny has produced no measurable evidence of chromium platelet spalling due to cracking in the plane of the chromium plate/gun steel interface.

Below is a detailed summary of our hot gas erosion theory and its relationship to the above calculations and empirical data. Equation (1) depicts the A723 gun steel/HC chromium plate interface as-plated (left) and with in-progress interface degradation (right). Nonequilibrium HC chromium plate shrinks and cracks widen by thermal repacking and out-gassing. The vertical dashed line is one side of a radial crack wall. The first chromium plated interface layer and the iron degradation layer are actually multiple atomic layers. Gun steel interface degradation is dominated by the recurring formation and removal of a thin surface layer of measurable untempered martensite, a thin surface layer of measurable oxidation, a somewhat thicker layer of measurable interstitially diffused carbon, and theoretically a thicker layer of unmeasurable interstitially diffused hydrogen. Oxidation of gun steel wall iron can occur in a moderately reducing combustion gas environment, since oxygen has more of an affinity for this iron metal than it does for partially oxidized gas species. The chromium/gun steel interface and the resultant gun steel interface surface produced by interface degradation are in excess of ninety-five percent iron and are at higher energy and more susceptible to damage from oxygen, carbon, and hydrogen than the bulk iron. High concentrations of damaging oxygen and carbon products have been measured at the iron interface. In addition, carbon and hydrogen products diffuse into and embrittle the gun steel.

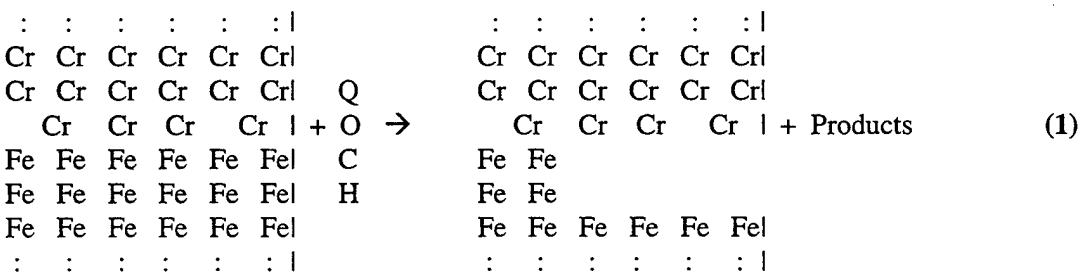

Metal-metal bonds have an equilibrium energy balance between attractive and repulsive forces that determines the activation energy necessary to break these bonds. If the local system energy increases, then this activation energy is easier to achieve.

Our gun erosion code wall heat transfer and wall temperature model has provided the following information:

- Bore surface temperatures for chromium plate and exposed gun steel (after chromium platelet spalling) from turbulent convection
- Radial crack wall surface and interface temperatures for chromium plate and gun steel from turbulent convection and conduction
- Bore surface and chromium/gun steel interface temperatures away from a radial crack for chromium plate and gun steel from conduction alone

At the 0.6 to 1.2 meter region, the chromium/gun steel interface, resultant gun steel interface surface due to interface degradation, and resultant gun steel surface due to chromium spalling typically exhibit deep radial crack depth and little erosion. The minimal erosion is mainly attributed to gun steel interface degradation, although less than five percent is attributed to radial crack linkage erosion. At this region, gas pressure is high, gas temperature is high, gas velocity is low, the boundary layer is thick, subsurface exposure is moderate, hot gas convective heat transfer is mildly turbulent at the surface, hot gas convective heat transfer is nonturbulent in the axial direction radial cracks, and hot gas convective heat transfer is nonturbulent in the circumferential direction radial cracks. These conditions allow conductive heating to dominate the gun steel interface temperature values at the radial crack walls. For this region, the respective relationships between the gas, surface, and crack wall interface temperatures are ~1.0x, ~0.6x, and ~0.3x.

At the 1.2 to 2.4 meter region, the chromium/gun steel interface, resultant gun steel interface surface due to interface degradation, and resultant gun steel surface due to chromium spalling typically exhibit moderate radial crack depth and mild erosion. This erosion is mainly attributed to gun steel interface degradation, although less than five percent is attributed to radial crack linkage erosion. At this region, gas pressure is moderate, gas temperature is moderate, gas velocity is high, the boundary layer is thin, subsurface exposure is high, hot gas convective heat transfer is moderately turbulent at the surface, hot gas convective heat transfer is mildly turbulent in the axial direction radial cracks, and hot gas convective heat transfer is nonturbulent in the circumferential direction radial cracks. These conditions allow convective heating to dominate the gun steel interface temperature values at the radial crack walls. For this region, the respective relationships between the gas, surface, and crack wall interface temperatures are ~1.0x, ~0.6x, and ~0.5x. Conduction alone into the wall away from the radial crack wall surface is a bad indicator of erosion, since it ignores the important turbulent convective element at the radial crack wall surface.

Figure 6 shows the M256/M829 MACE wall temperature profile analysis for HC chromium maximum surface temperature (T_{wall}) as a function of round-conditioning temperatures for selected axial positions. The HC chromium maximum T_{wall} is about 1600°K, which is below its passivating oxidation temperature at about 2000°K, and well below its melting point at about 2130°K, thus explaining its inertness.

Figure 7 shows the M256/M829 MACE wall temperature profile analysis for A723 maximum interface and surface wall temperatures (T_{wall}) as a function of round-conditioning temperatures for selected axial positions. The A723 maximum interface T_{wall} values are a combination of convection and conduction at the crack walls. The A723/iron maximum interface T_{wall} is about 1225°K, which is above its rapid expansive flaking oxidation temperature at about 1055°K, explaining its reactivity. In addition, it is below its iron oxide melting point at about 1640°K and well below its A723/iron melting point at about 1810°K. Diffusion, reactions, transformations, and gas wash thermochemically degrade interfacial A723 at HC chromium plate

heat-checked crack bases. The A723/iron maximum surface T_{wall} is about 1375°K, which is well above its rapid expansive flaking oxidation temperature at about 1055°K, explaining its reactivity. In addition, it is below its iron oxide melting point at about 1640°K and well below its A723/iron melting point at about 1810°K. Diffusion, reactions, transformations, and gas wash thermochemically degrade fully exposed surface A723 after HC chromium plate spalling.

Figures 6 and 7 show that wall temperature profiles follow the positional order of the heat transfer pattern from Figure 2. In these two figures, maximum values were used instead of time-dependent data to simplify their appearance. Also, experimental thermal repacking depth away from cracks, thermal transformation depth away from cracks, and thermocouple data were used to calibrate calculated wall temperature profiles.

Figure 8 summarizes the M256/M829 MACE cumulative erosion analysis for the unrealistic, but informative case of only 49°C conditioned rounds as a function of cumulative rounds for selected axial positions. The figure shows the 2.18 meter axial position to be the most eroded position. It takes about 140 rounds for chromium platelet spalling onset/gun steel gas wash onset to occur, and it takes about 510 rounds to achieve the 5 mm of cumulative erosion required to condemn this gun for erosion.

Figure 9 summarizes the M256/M829 MACE cumulative erosion analysis for the unrealistic, but informative case of only 21°C conditioned rounds as a function of cumulative rounds for selected axial positions. The figure shows the 2.18 meter axial position to be the most eroded position. It takes about 225 rounds for chromium platelet spalling onset/gun steel gas wash onset to occur, and it takes about 770 rounds to achieve the 5 mm of cumulative erosion required to condemn this gun for erosion.

Figure 10 summarizes the M256/M829 MACE cumulative erosion analysis for the unrealistic, but informative case of only -32°C conditioned rounds as a function of cumulative rounds for selected axial positions. The figure shows the 2.18 meter axial position to be the most eroded position. It takes about 325 rounds for chromium platelet spalling onset/gun steel gas wash onset to occur, and it takes about 1150 rounds to achieve the 5 mm of cumulative erosion required to condemn this gun for erosion.

Figure 11 summarizes the M256/M829 MACE cumulative erosion analysis for the semi-realistic and informative case of an equal distribution of hot/ambient/cold-conditioned rounds as a function of cumulative rounds for selected axial positions. This figure also shows the 2.18 meter axial position to be the most eroded position. It takes about 180 rounds for chromium platelet spalling onset/gun steel gas wash onset to occur, and it takes about 720 rounds to achieve the 5 mm of cumulative erosion required to condemn this gun for erosion.

Figures 8 through 11 show that cumulative wall erosion profiles also follow the positional order of the heat transfer pattern from Figure 2. Erosion life is lowest at 2.18 meters, higher at 1.55 meters, still higher at 0.69 meter, higher yet at 3.30 meters, and highest at 5.11 meters from RFT. Additionally, these four figures also that interface life follows this same pattern with the exception of the 5.11 meter position, which is believed to be by a different mechanism.

The erosion mechanism consists of:

- Heat checking of the inert chromium plate
- Subsequent interfacial degradation of the subsurface gun steel substrate at the chromium crack bases
- Subsequent chromium platelet spalling
- Subsequent bare gun steel gas wash

Mechanisms of interface degradation include diffusion, reactions (i.e., expansive oxidation), transformations, and gas wash. This overall gun erosion analysis correctly predicts that the worst eroded region is located at 1.2 to 2.4 meters from RFT. The excessive gas wash-free muzzle wear is by a different purely mechanical mechanism. Our overall gun erosion analysis correctly predicts the following relative distribution of M256 erosion-related effective full-charge values: if M829 at -32°C = 1.0, then M829 at 21°C = 1.5, M829 at 49°C = 2.2, M829A1 at -32°C =1.3, M829A1 at 21°C = 1.9, M829A1 at 49°C = 2.8, M829A2 at -32°C =1.5, M829A2 at 21°C = 2.3, and M829A2 at 49°C = 3.4. Traditionally, all M256 effective full-charge values have been equal to one per the U.S. Army Evaluation of Cannon Tubes Technical Manual.

REFERENCES

1. Alkidas, A., Morris, S., Christoe, C., Caveny, L., and Summerfield, M., "Erosive Effects of Various Pure and Combustion-Generated Gases on Metals - Part II," U.S. Army Materials and Mechanics Research Center, Watertown, MA, 1977; see also Part I, 1975.

2. Picard, J., Ahmad, I., and Bracuti, A., *Proceedings of the Tri-Service Gun Tube Wear and Erosion Symposiums*, U.S. Army ARDEC/ADPA, Dover, NJ, 1970, 1972, 1977, and 1982.

3. Dunn, S., Sopok, S., Coats, D., O'Hara, P., Nickerson, G., and Pflegl, G., "Unified Computer Model for Predicting Thermochemical Erosion in Gun Barrels," *Proceedings of 31st AIAA Propulsion Conference*, San Diego, CA, July 1995.

4. Gough, P., "The XNOVAKTC Code," Paul Gough Associates, Portsmouth, NH, 1990.

5. Corner, J., *Theory of the Interior Ballistics of Guns*, John Wiley and Sons, New York, 1950.

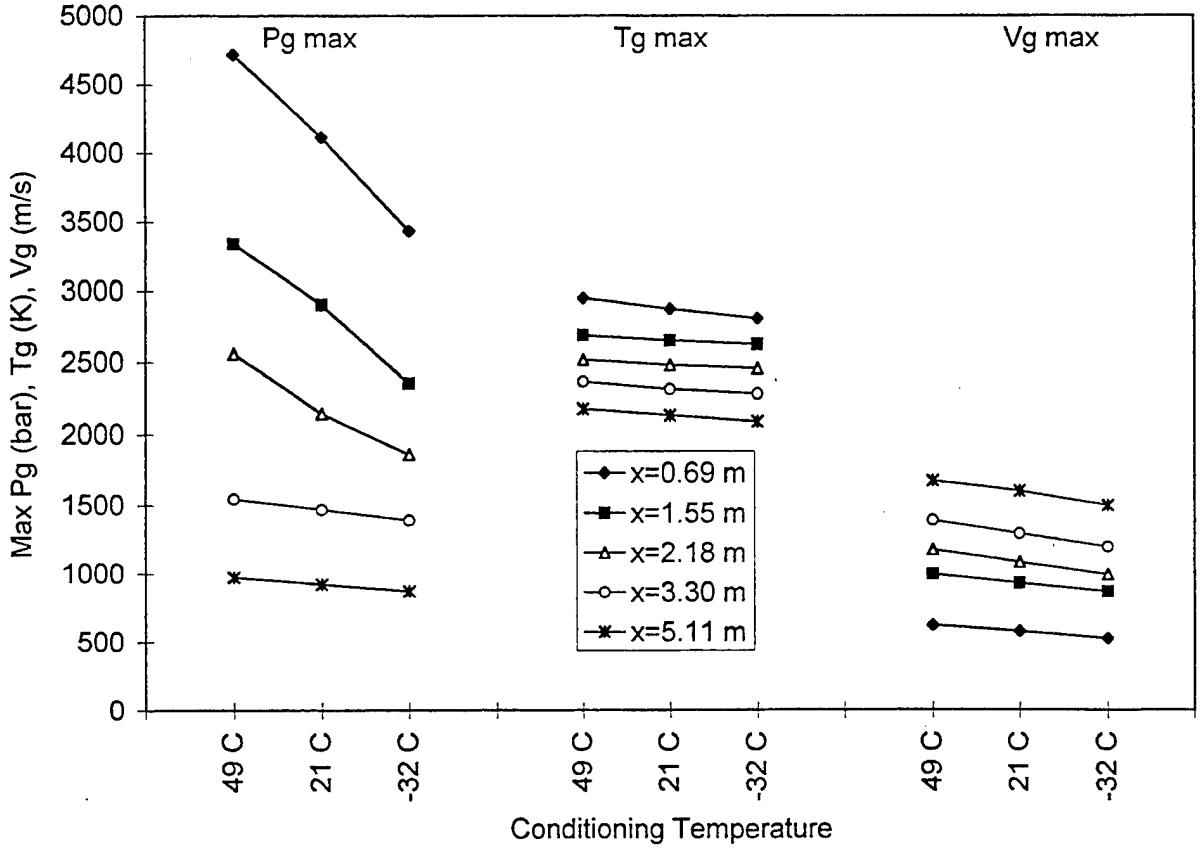

Figure 1. M829 calibrated XNOVAKTC interior ballistic analysis for maximum values of gas pressure, gas temperature, and gas velocity.

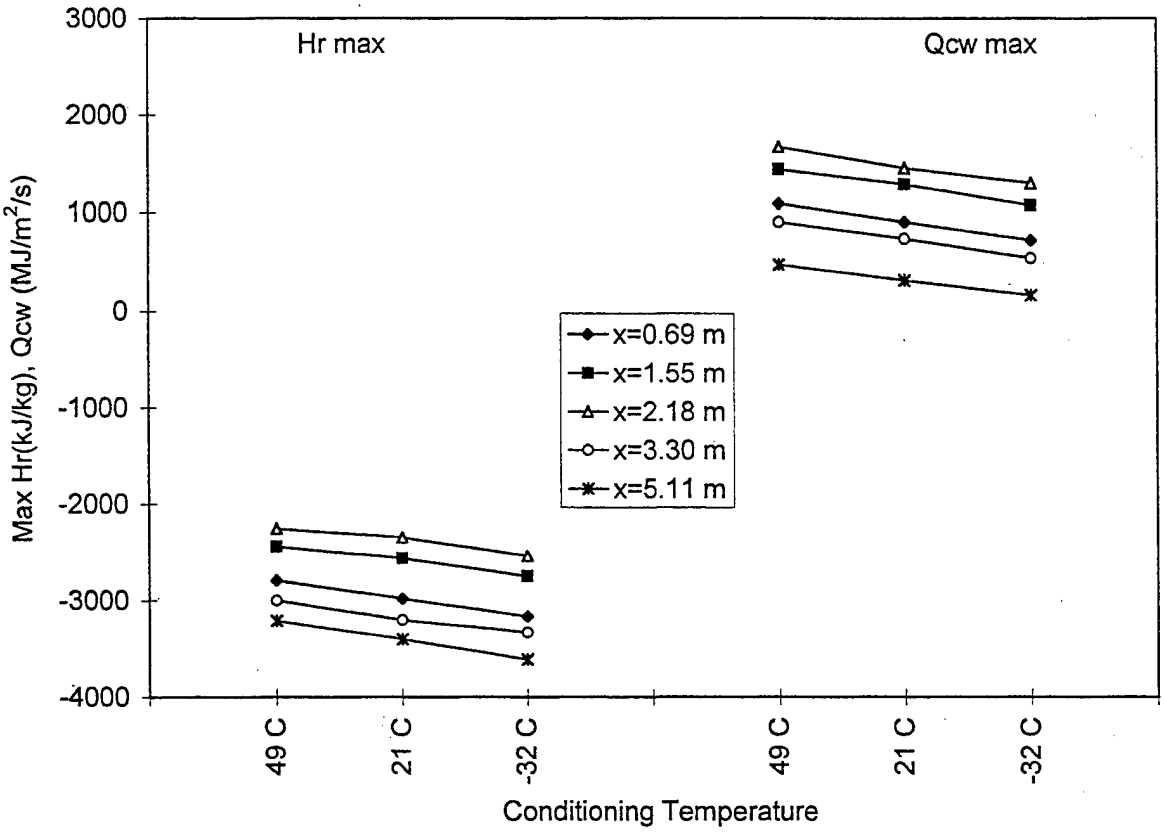

Figure 2. M829 calibrated MABL analysis for maximum values of recovery enthalpy and cold wall heat flux.

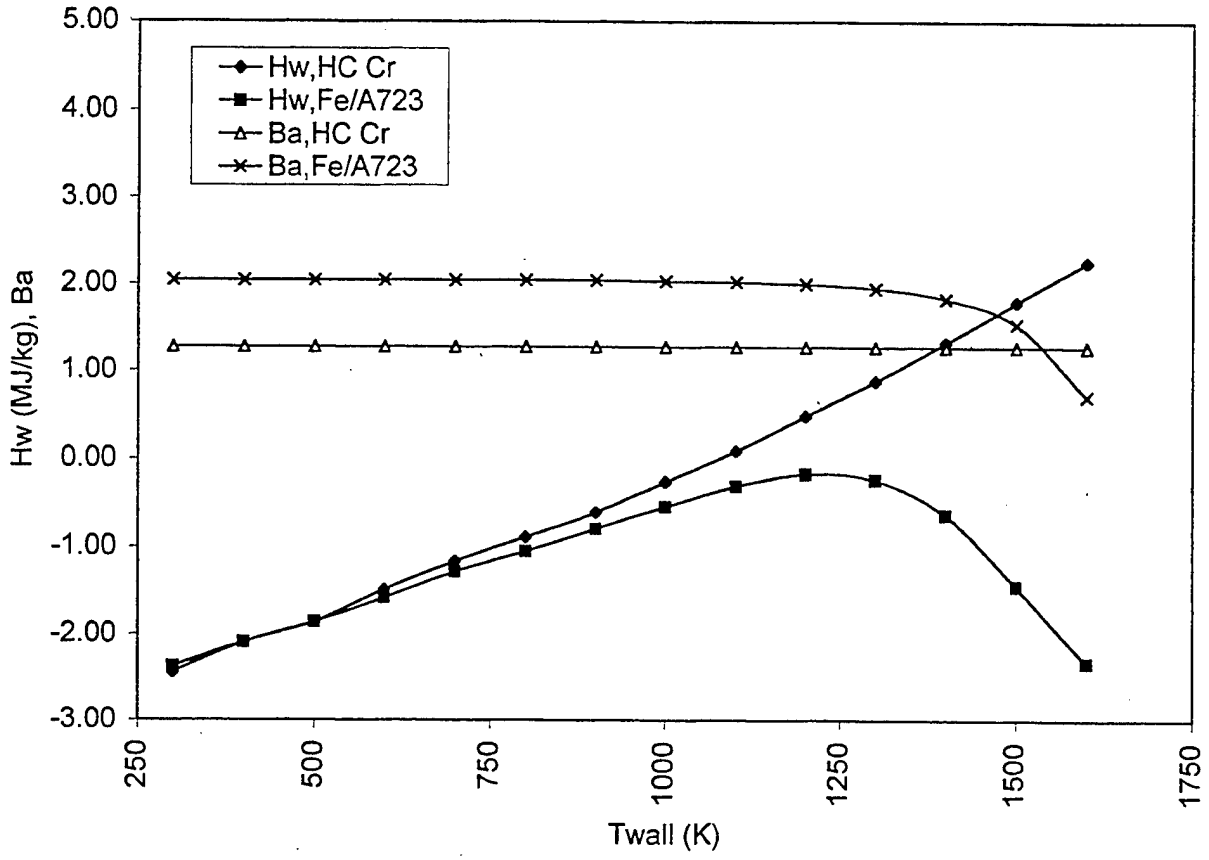

Figure 3. M829 calibrated CCET thermochemical analysis of reacting wall enthalpy and ablation potential.

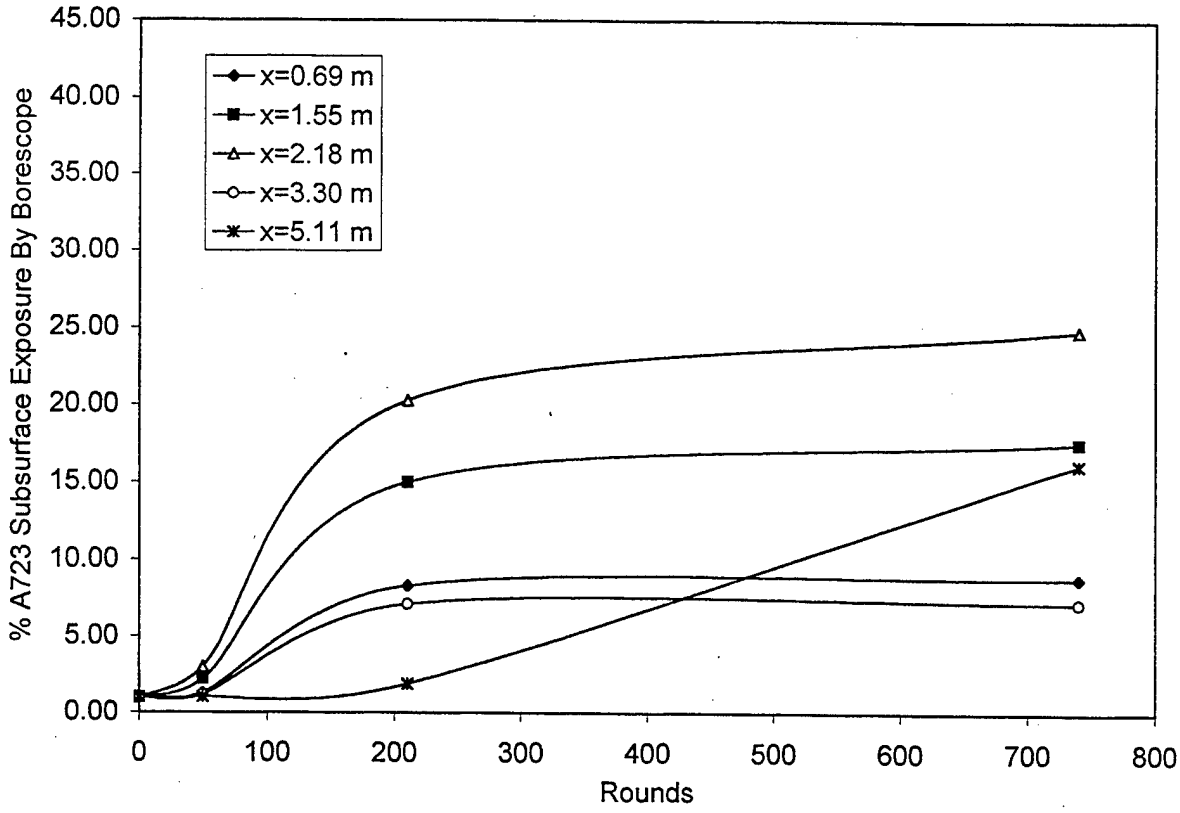

Figure 4. M829 borescope data analysis of the A723 subsurface exposure through HC chromium plate cracks.

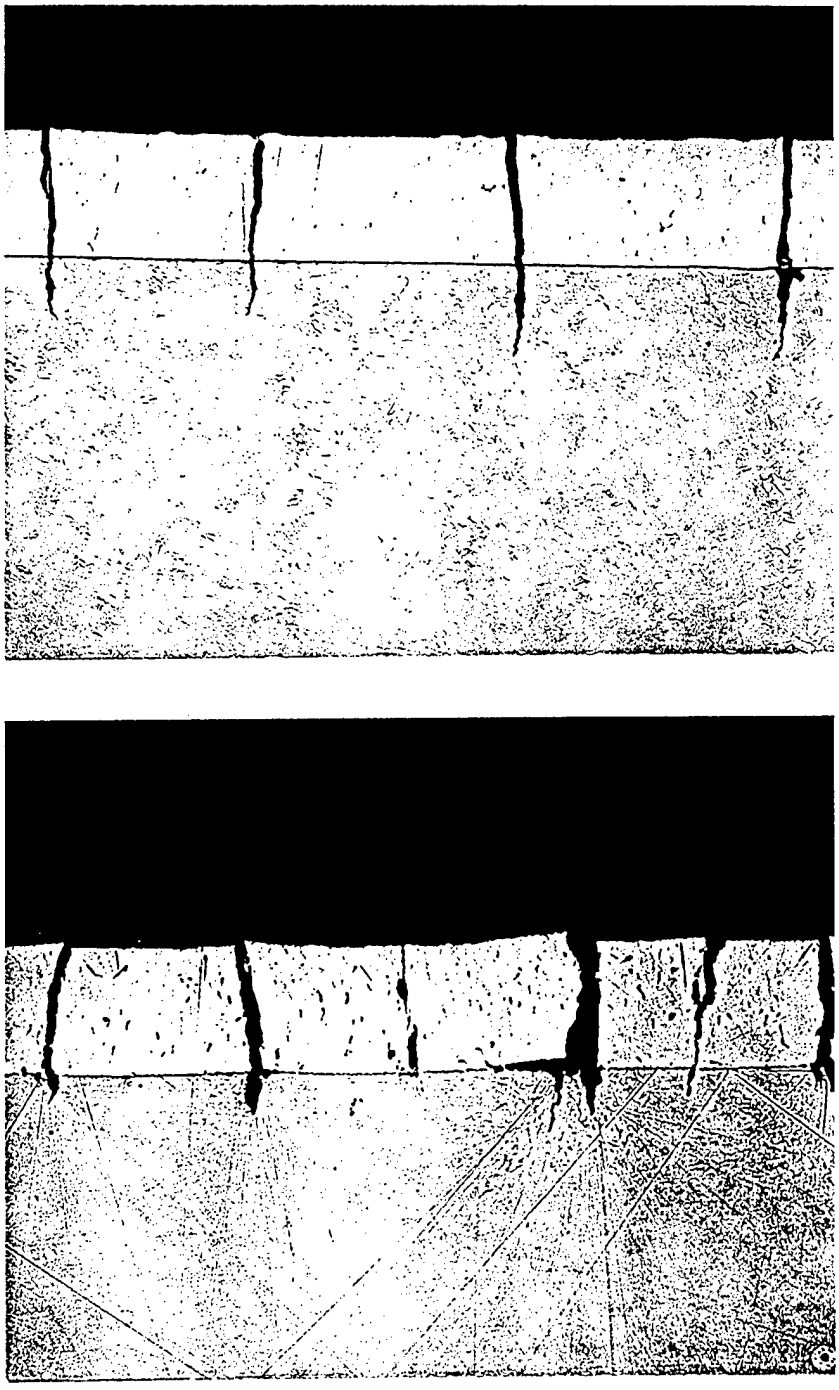

Figure 5. M829 metallographs at 0.69 meter representing 0.6 to 1.2 meter region (top) and at 1.55 meters representing 1.2 to 2.4 meter region (bottom).

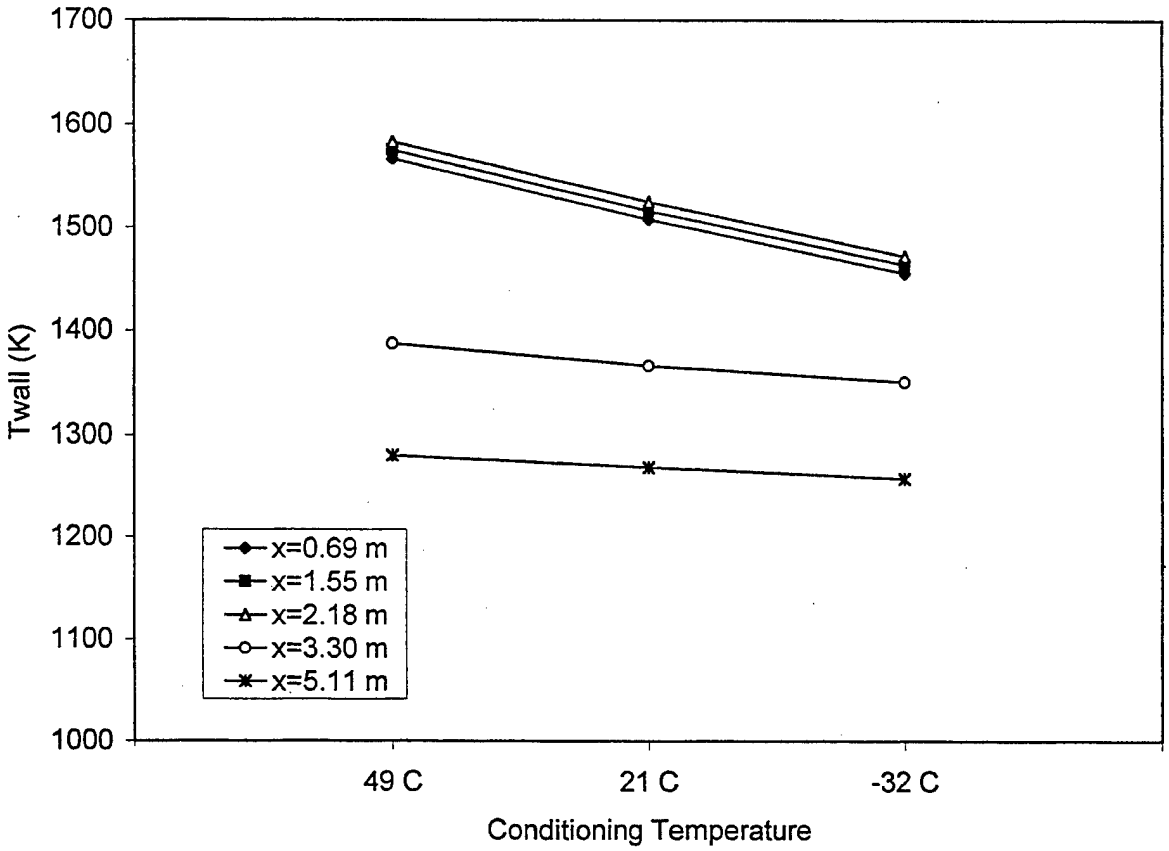

Figure 6. M256/M829 calibrated MACE wall temperature profile analysis for HC chromium maximum surface temperature.

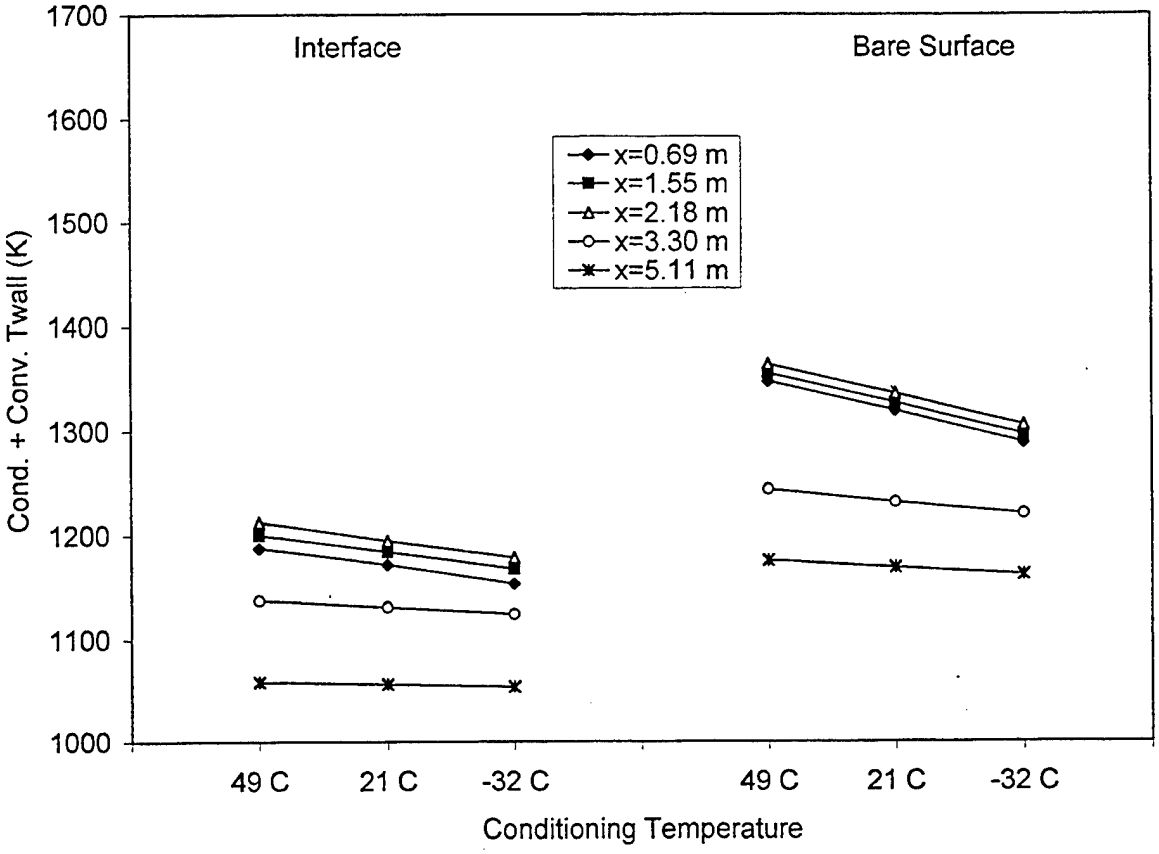

Figure 7. M256/M829 calibrated MACE wall temperature profile analysis for A723 maximum interface and surface wall temperatures.

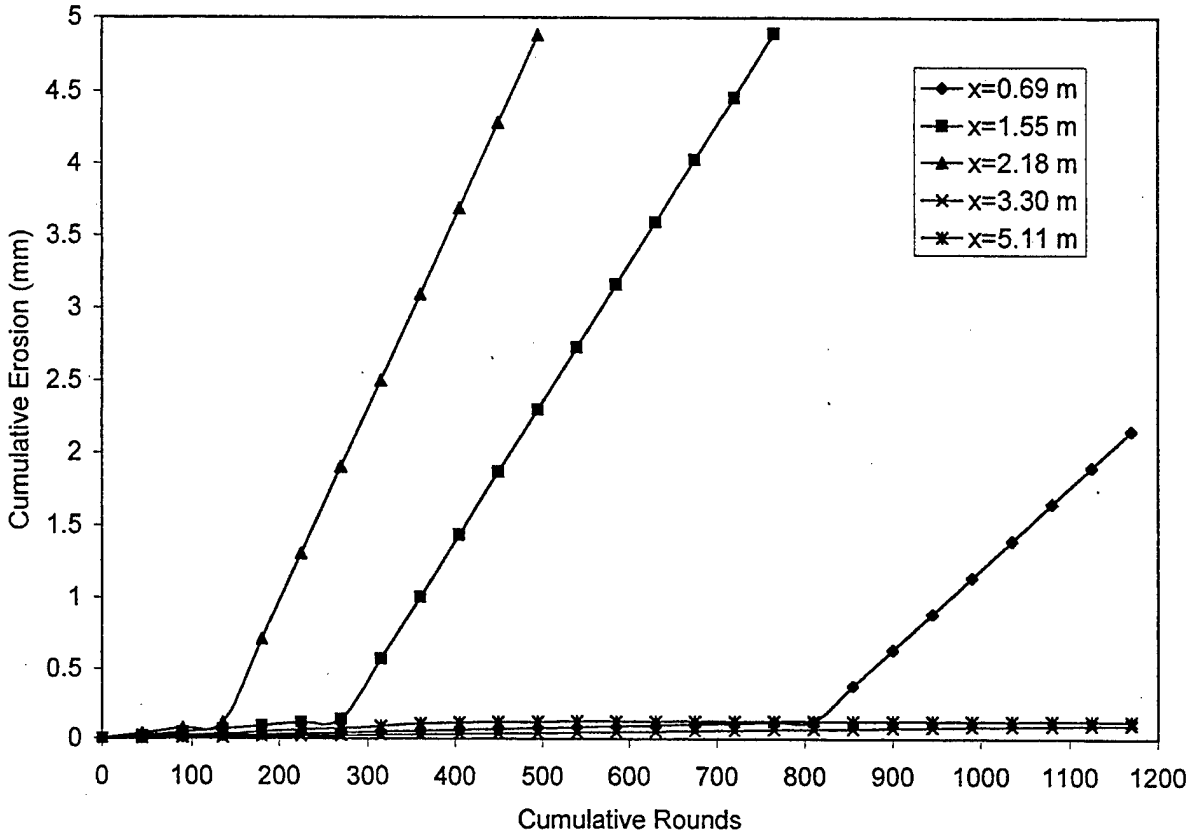

Figure 8. M256/M829 MACE cumulative erosion analysis for the unrealistic, but informative case of only 49°C conditioned rounds.

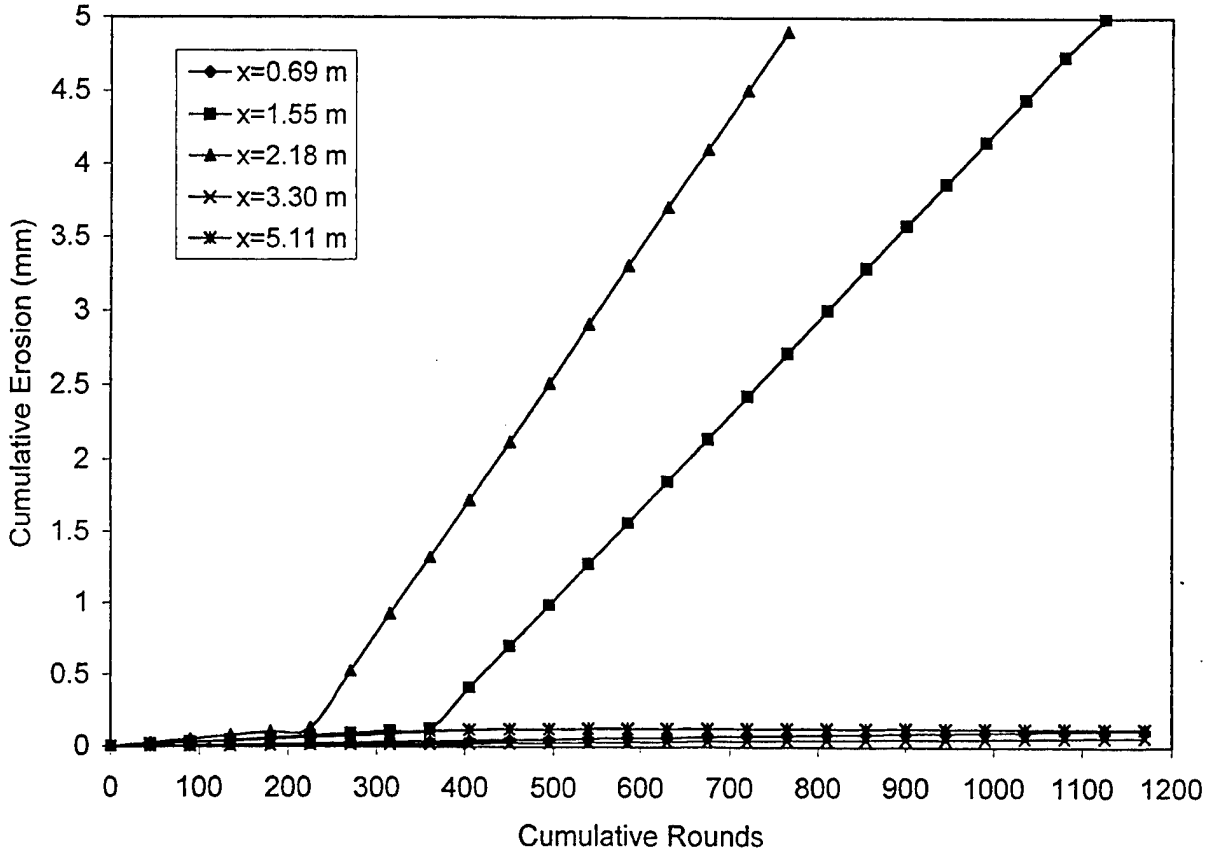

Figure 9. M256/M829 MACE cumulative erosion analysis for the unrealistic, but informative case of only 21°C conditioned rounds.

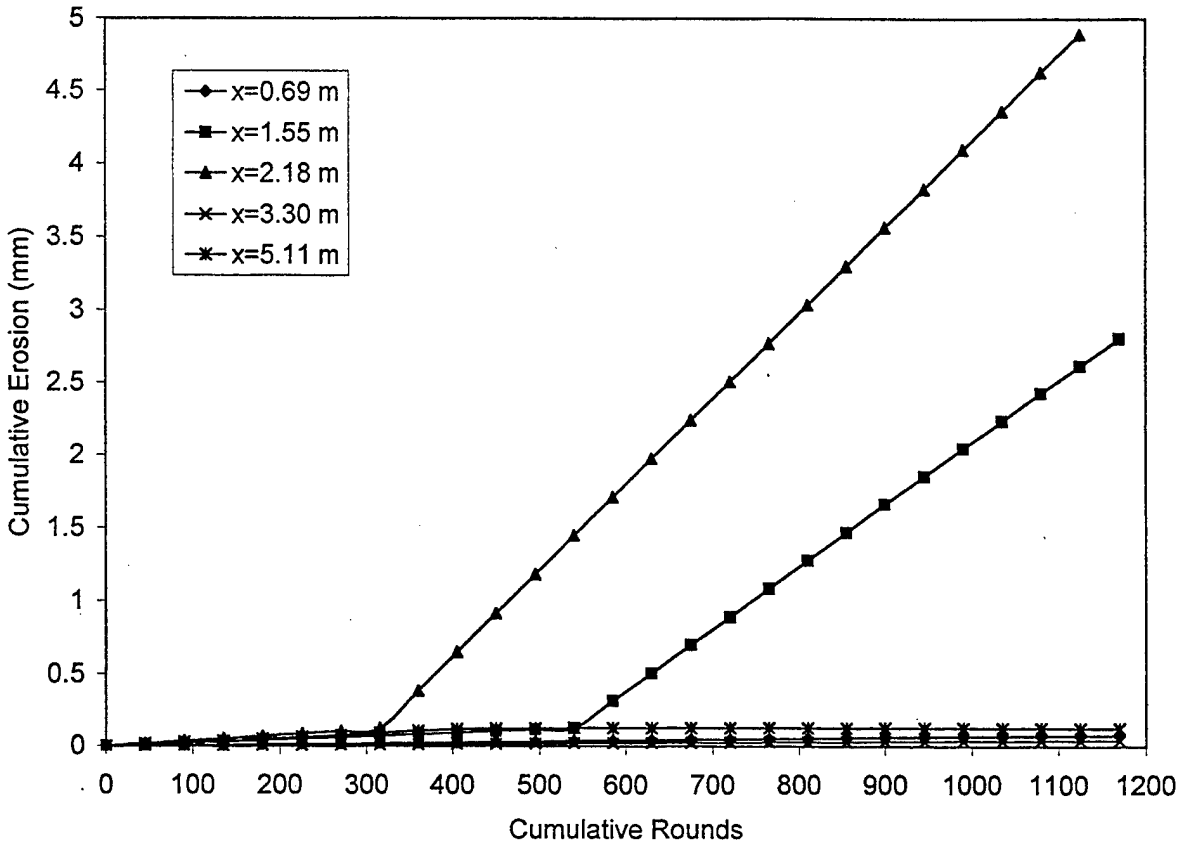

Figure 10. M256/M829 MACE cumulative erosion analysis for the unrealistic, but informative case of only -32°C conditioned rounds.

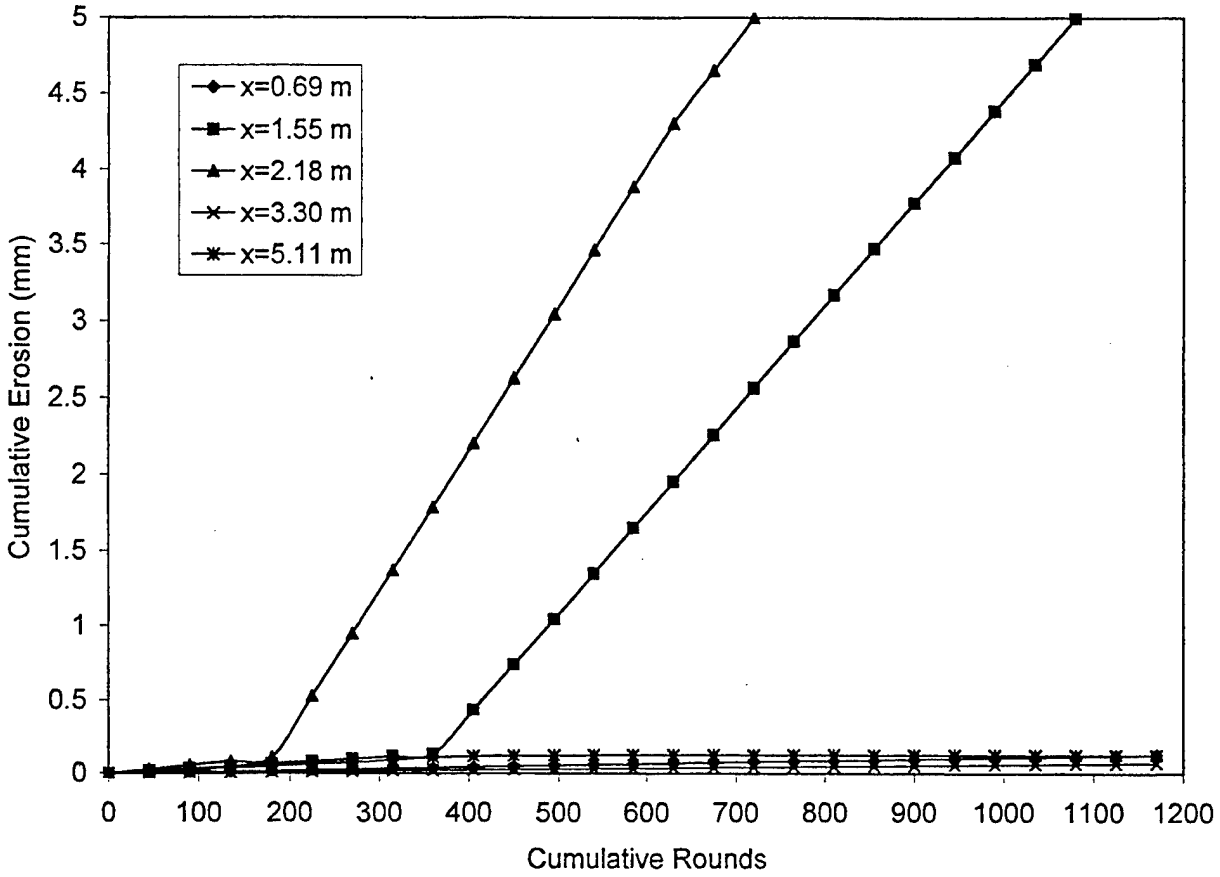

Figure 11. M256/M829 MACE cumulative erosion analysis for the semi-realistic and informative case of an equal distribution of hot/ambient/cold-conditioned rounds.

TECHNICAL REPORT INTERNAL DISTRIBUTION LIST

	NO. OF COPIES
CHIEF, DEVELOPMENT ENGINEERING DIVISION	
ATTN: AMSTA-AR-CCB-DA	1
-DB	1
-DC	1
-DD	1
-DE	1
CHIEF, ENGINEERING DIVISION	
ATTN: AMSTA-AR-CCB-E	1
-EA	1
-EB	1
-EC	1
CHIEF, TECHNOLOGY DIVISION	
ATTN: AMSTA-AR-CCB-T	2
-TA	1
-TB	1
-TC	1
TECHNICAL LIBRARY	
ATTN: AMSTA-AR-CCB-O	5
TECHNICAL PUBLICATIONS & EDITING SECTION	
ATTN: AMSTA-AR-CCB-O	3
OPERATIONS DIRECTORATE	
ATTN: SIOWV-ODP-P	1
DIRECTOR, PROCUREMENT & CONTRACTING DIRECTORATE	
ATTN: SIOWV-PP	1
DIRECTOR, PRODUCT ASSURANCE & TEST DIRECTORATE	
ATTN: SIOWV-QA	1

NOTE: PLEASE NOTIFY DIRECTOR, BENÉT LABORATORIES, ATTN: AMSTA-AR-CCB-O OF ADDRESS CHANGES.

TECHNICAL REPORT EXTERNAL DISTRIBUTION LIST

	NO. OF COPIES
DEFENSE TECHNICAL INFO CENTER ATTN: DTIC-OCA (ACQUISITIONS) 8725 JOHN J. KINGMAN ROAD STE 0944 FT. BELVOIR, VA 22060-6218	2
COMMANDER U.S. ARMY ARDEC ATTN: AMSTA-AR-WEE, BLDG. 3022 AMSTA-AR-AET-O, BLDG. 183 AMSTA-AR-FSA, BLDG. 61 AMSTA-AR-FSX AMSTA-AR-FSA-M, BLDG. 61 SO AMSTA-AR-WEL-TL, BLDG. 59 PICATINNY ARSENAL, NJ 07806-5000	 1 1 1 1 1 2
DIRECTOR U.S. ARMY RESEARCH LABORATORY ATTN: AMSRL-DD-T, BLDG. 305 ABERDEEN PROVING GROUND, MD 21005-5066	 1
DIRECTOR U.S. ARMY RESEARCH LABORATORY ATTN: AMSRL-WM-MB (DR. B. BURNS) ABERDEEN PROVING GROUND, MD 21005-5066	 1
COMMANDER U.S. ARMY RESEARCH OFFICE ATTN: TECHNICAL LIBRARIAN P.O. BOX 12211 4300 S. MIAMI BOULEVARD RESEARCH TRIANGLE PARK, NC 27709-2211	 1
COMMANDER ROCK ISLAND ARSENAL ATTN: SIORI-SEM-L ROCK ISLAND, IL 61299-5001	 1
COMMANDER U.S. ARMY TANK-AUTMV R&D COMMAND ATTN: AMSTA-DDL (TECH LIBRARY) WARREN, MI 48397-5000	 1
COMMANDER U.S. MILITARY ACADEMY ATTN: DEPT OF CIVIL & MECH ENGR WEST POINT, NY 10966-1792	 1
U.S. ARMY AVIATION AND MISSILE COM REDSTONE SCIENTIFIC INFO CENTER ATTN: AMSAM-RD-OB-R (DOCUMENTS) REDSTONE ARSENAL, AL 35898-5000	 2
COMMANDER U.S. ARMY FOREIGN SCI & TECH CENTER ATTN: DRXST-SD 220 7TH STREET, N.E. CHARLOTTESVILLE, VA 22901	 1

NOTE: PLEASE NOTIFY COMMANDER, ARMAMENT RESEARCH, DEVELOPMENT, AND ENGINEERING CENTER, BENÉT LABORATORIES, CCAC, U.S. ARMY TANK-AUTOMOTIVE AND ARMAMENTS COMMAND, AMSTA-AR-CCB-O, WATERVLIET, NY 12189-4050 OF ADDRESS CHANGES.